



## Electrostatics of metal-graphene interfaces: sharp p-n junctions for electron-optical applications

Cherves, Ferney A.; Jiménez, David; Santos, Jaime E.; Bøggild, Peter; Caridad, Jose M.

*Published in:*  
Nanoscale

*Link to article, DOI:*  
[10.1039/C9NR02029B](https://doi.org/10.1039/C9NR02029B)

*Publication date:*  
2019

*Document Version*  
Peer reviewed version

[Link back to DTU Orbit](#)

*Citation (APA):*  
Cherves, F. A., Jiménez, D., Santos, J. E., Bøggild, P., & Caridad, J. M. (2019). Electrostatics of metal-graphene interfaces: sharp p-n junctions for electron-optical applications. *Nanoscale*, 11(21), 10273-10281.  
<https://doi.org/10.1039/C9NR02029B>

---

### General rights

Copyright and moral rights for the publications made accessible in the public portal are retained by the authors and/or other copyright owners and it is a condition of accessing publications that users recognise and abide by the legal requirements associated with these rights.

- Users may download and print one copy of any publication from the public portal for the purpose of private study or research.
- You may not further distribute the material or use it for any profit-making activity or commercial gain
- You may freely distribute the URL identifying the publication in the public portal

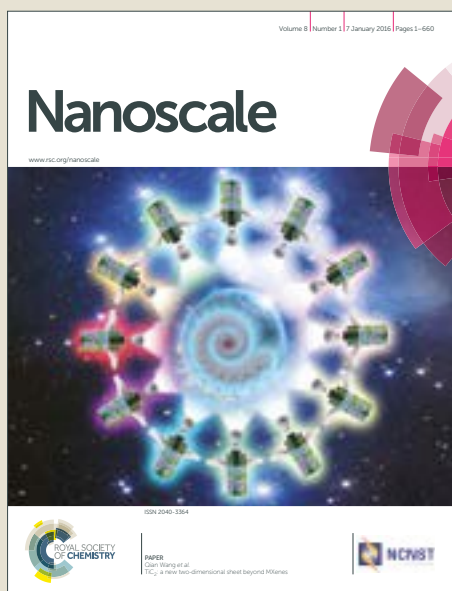
If you believe that this document breaches copyright please contact us providing details, and we will remove access to the work immediately and investigate your claim.

# Nanoscale

Accepted Manuscript



This article can be cited before page numbers have been issued, to do this please use: F. A. Chaves, D. Jiménez, J. E. Santos, P. Bøggild and J. M. Caridad, *Nanoscale*, 2019, DOI: 10.1039/C9NR02029B.



This is an Accepted Manuscript, which has been through the Royal Society of Chemistry peer review process and has been accepted for publication.

Accepted Manuscripts are published online shortly after acceptance, before technical editing, formatting and proof reading. Using this free service, authors can make their results available to the community, in citable form, before we publish the edited article. We will replace this Accepted Manuscript with the edited and formatted Advance Article as soon as it is available.

You can find more information about Accepted Manuscripts in the [author guidelines](#).

Please note that technical editing may introduce minor changes to the text and/or graphics, which may alter content. The journal's standard [Terms & Conditions](#) and the ethical guidelines, outlined in our [author and reviewer resource centre](#), still apply. In no event shall the Royal Society of Chemistry be held responsible for any errors or omissions in this Accepted Manuscript or any consequences arising from the use of any information it contains.

# Electrostatics of metal-graphene interfaces: sharp $p$ - $n$ junctions for electron-optical applications

Ferney A. Chaves<sup>1</sup>, David Jiménez<sup>1</sup>, Jaime E. Santos<sup>2</sup>, Peter Bøggild<sup>3</sup>, José M. Caridad<sup>3†</sup>

<sup>1</sup>*Department d'Enginyeria Electrònica, Escola d'Enginyeria, Campus UAB, Bellaterra, 08193  
Barcelona, Spain*

<sup>2</sup>*Centro de Física and Departamento de Física, Universidade do Minho, P-4710-057 Braga,  
Portugal*

<sup>3</sup>*Center for Nanostructured Graphene (CNG), Department of Physics, Technical University of  
Denmark, 2800 Kongens Lyngby, Denmark*

†corresponding author: [jcar@dtu.dk](mailto:jcar@dtu.dk)

**Keywords:** graphene, electron optics, sharp pn junctions, metal-graphene interfaces

**ABSTRACT.**

Creation of sharp lateral  $p$ - $n$  junctions in graphene devices, with transition widths  $w$  well below the Fermi wavelength  $\lambda_F$  of graphene's charge carriers, is vital to study and exploit these electronic systems for electron-optical applications. The achievement of such junctions is, however, not trivial due to the presence of a considerable out-of-plane electric field in lateral  $p$ - $n$  junctions, resulting in large widths. Metal-graphene interfaces represent a novel, promising and easy to implement technique to engineer such sharp lateral  $p$ - $n$  junctions in graphene field-effect devices, in clear contrast to the much wider (i.e. smooth) junctions achieved via conventional local gating. In this work, we present a systematic and robust investigation of the electrostatic problem of metal-induced lateral  $p$ - $n$  junctions in gated

graphene devices for electron-optics applications, systems where the dependence of the width  $w$  of the created junctions is not only determined by the metal used but also on external factors such as device geometries, dielectric environment and different operational parameters such as carrier density and temperature. Our calculations demonstrate that sharp junctions ( $w \ll \lambda_F$ ) can be achieved via metal-graphene interfaces at room temperature in non-encapsulated devices surrounded by dielectric media with low relative permittivity ( $<10$ ). In addition, we show how specific details such as the separation distance between metal and graphene and the permittivity of the gap in-between plays a critical role when defining the p-n junction, not only defining its width  $w$  but also the energy shift of graphene underneath the metal. These results can be extended to any two-dimensional (2D) electronic system doped by the presence of metal clusters and thus are relevant for understanding interfaces between metals and other 2D materials.

## 1. Introduction.

*Sharp lateral p-n junctions in graphene for electron optics applications.*

Electronic  $p-n$  junctions are well-known, fundamental constituents of current semiconductor technology, enabling, for instance, the control of current flow passing through devices such as diodes and transistors or allowing photoelectric conversion in solar cells. [1] These junctions are formed at the interface between two differently doped semiconductor regions or materials, one with excess of holes ( $p$ -type doped) and one with excess of electrons ( $n$ -type doped), where a built-in potential gradient across such  $p-n$  boundary is the actual responsible for the rectification of currents or the separation of photo-generated electron-hole pairs. The advent of semiconducting two-dimensional (2D) crystals has revived interest in studying  $p-n$  junctions from both fundamental and an applications' point of view. [2-4]. To a large extent, this is due to the unique possibility of

creating lateral, in-plane  $p$ - $n$  junctions of similar or different polarity ( $n$ - $n'$ ,  $n$ - $p$ ,  $p$ - $n$  and  $p$ - $p'$ ) in these semiconducting 2D systems [3-7]: being formed at the one-dimensional interface between two coplanar 2D regions, lateral  $p$ - $n$  junctions do not have a 3D counterpart. In practical terms, these  $p$ - $n$  junctions offer attractive opportunities to realize diodes with large rectification ratios that can be modulated by a gate-voltage [8] or photodetectors with high responsivity [9]. Moreover, lateral  $p$ - $n$  junctions in ballistic 2D electron systems enable the creation of novel and exciting device concepts based on the possibility to steer the electron flow at these interfaces analogously to the way optical lenses and prisms direct light in an optical apparatus.[10-15]

Among all potential candidates, graphene is arguably the most alluring 2D solid-state system to study and implement electron optics devices based on lateral  $p$ - $n$  junctions (Fig. 1a) due to several reasons. First, it displays ballistic transport over micrometer length scales even at room temperature [16,17], relevant for applications. In addition, being a zero-gap material with a linear dispersion relation makes graphenes' lateral  $p$ - $n$  junctions to be, in principle, highly transparent interfaces that support both conventional and negative electron refraction [13,14,18]. Not only that, the transmission probability  $T_{pn}$  across graphene  $p$ - $n$  junctions, which is theoretically determined by chiral (Klein) tunneling processes occurring at these interfaces, strongly depends on both the incident angle of the electron beam  $\theta$  [19] and the width of these  $p$ - $n$  junctions  $w$  (Fig.1a) [20,21].

For a symmetric and bipolar  $p$ - $n$  junction with a potential having a linear profile at the  $p$ - $n$  interface,

$T_{pn}$  at a specific electron Fermi wavelength  $\lambda_F$  is given by the expression [14]  $T_{pn} \sim e^{-2\pi^2 w / \lambda_F \sin^2 \theta}$

(Fig 1.b). As a result, a broad range of novel electron-optics devices with different functionalities can be implemented in graphene by appropriate choices of  $p$ - $n$  geometries (i.e  $\theta$  and curvature), and the junction width  $w$ . Such systems range from electron guiding devices [11,13-15] or beam collimators [22] to unconventional (Klein-tunneling) transistors employing the angle-dependent tunneling of Dirac electrons to engineer a gate-tunable current modulation in graphene [23-25].

Also, more sophisticated architectures such as two-dimensional Dirac fermion microscopes could be conceived by designing spatial arrangements of source-drain contacts and  $p$ - $n$  junctions in graphene similar to the arrangement of electron sources, detectors and optics in an electron microscope [26,27]. The basic design principles for graphene's  $p$ - $n$  interfaces are two [20-22]: *i*) sharp  $p$ - $n$  junctions where  $w$  is much smaller than  $\lambda_F$  (case  $w/\lambda_F \ll 1$ ) allow a relatively wide range of incoming angles to be transmitted. These highly transparent interfaces allow the realization of the so-called Veselago lenses, capable of focusing diverging trajectories of electrons emanating from a point source (Fig. 1c). *ii*) smooth  $p$ - $n$  junctions (case  $w/\lambda_F > 1$ ) represent interfaces where only electrons near normal incidence are transmitted while the rest are reflected, acting as electron beam (Klein) collimators (Fig. 1d). Considering typical carrier densities  $n$  in graphene devices below  $3 \times 10^{12} \text{ cm}^{-2}$  [11-15]; the condition of sharp  $p$ - $n$  junction is fulfilled for widths  $w \ll \lambda_F = 2\sqrt{\pi/n} \approx 20 \text{ nm}$ , i.e. for  $w$  below 10 nm. For completeness, we note that sharp (and therefore smooth) lateral  $p$ - $n$  junctions should additionally vary softly with respect to the lattice scale of graphene  $a$  in electron-optics devices (i.e.  $w \gg a \sim 0.2 \text{ nm}$ ) to avoid inter-valley scattering in the system [21]. Thus, one can establish an approximated interval for useful, sharp lateral  $p$ - $n$  junctions in graphene for junction widths  $0.5 \leq w \leq 10 \text{ nm}$ .

#### *Implementing sharp lateral $p$ - $n$ junctions in graphene field-effect devices.*

From a technological perspective, sharp lateral  $p$ - $n$  junctions are the key elements to achieve practical devices based on electron-optics principles. This is not only due to their aforementioned outstanding focusing ability, their high transparency enables a much larger carrier modulation (or contrast [22]) in these interfaces compared to smooth junctions [21, 22]; a vital aspect for applications. However, the technical implementation of sharp lateral  $p$ - $n$  junctions in typical potential steps of the order of 0.1 eV [20-22] in graphene devices is highly challenging

[13,14,24,25]. This is due to the prominent out-of-plane electric field present around lateral  $p-n$  interfaces, consequence of the system dimensionality; together with the weak screening of charge carriers existing in 2D materials due to their low density of states, [3,6,7] both of which considerably contributes to increasing the junction size  $w$ .

For instance, junction widths  $w$  achieved via conventional local gating techniques such as bottom-, top- or split-gates are predominantly defined by the distance  $b$  between the graphene sheet and the gates [13,14,28], which depend on the thickness of the dielectric material. The realization of sharper junctions could be attempted in these multiple-gate devices by using thin top and bottom dielectric layers with  $b \leq 5\text{nm}$ . Yet, in practice, these ultrathin dielectric films are limited by possible defects and/or ultimately quantum tunneling [29-31], compromising the proper functioning of the device.

In clear contrast, metal islands of different geometries deposited on graphene offer an alternative opportunity to realize sharp lateral  $p-n$  junctions in this 2D material (Fig.2). This is due to two main reasons: *i*) metals can dope graphene due to both electron transfer and chemical interactions taking place at metal-graphene interfaces [32,33], enabling the creation of lateral  $p-n$  junctions in the 2D material and *ii*) provide partial screening of the out-of-plane electric field existent at these  $p-n$  interfaces, reducing thus the junction width  $w$ . Indeed, sharp  $p-n$  junctions with potential steps of  $\sim 0.1\text{ eV}$  and  $w \sim 1\text{ nm}$  have been measured via scanning tunneling microscopy (STM) in continuous graphene sheets placed on copper [34,35], where the differently doped graphene regions occur at the interface of copper surfaces having different surface potentials. Not only that, it has also been possible to observe *gate-controlled* electron guiding in graphene by placing periodic arrays of metal nano-dots on graphene *field-effect devices* [15]. The observation of such guiding phenomenon in multiple (cascaded)  $p-n$  junctions at room temperature [15] relies on the formation of sharp  $p-n$  junctions at metal-graphene interfaces, even under the remote influence of the back-gate. The justification of this assumption has not yet been verified, nor has its implications been examined,

and this is the main objective of this work. Whereas the existence of abrupt potential steps is generally assumed to occur at any metal-induced  $p$ - $n$  interface in graphene field-effect devices (including contact regions) [15,36-40], realistic calculations of such potential profiles have never been carried out. These calculations are needed to engineer electron optics, since the width  $w$  of such  $p$ - $n$  junctions will depend on device geometries, dielectric environments and/or working conditions. In the present study, we undertake a systematic and robust investigation of the electrostatic problem of metal-induced lateral  $p$ - $n$  junctions on graphene field-effect devices (i.e. accounting for the remote influence of the global back-gate) for electron-optics applications. Apart from the dependence on the carrier concentration  $n$  (i.e. Fermi level  $E_F$ ) and height of the potential barrier  $\Delta E$ , four additional key factors could produce a noticeable impact on  $w$ : *i*) separation distance between metal and graphene  $t_d$ ; *ii*) dielectric materials composing the device, including the possible presence of an ultra-thin dielectric at the actual metal-graphene interface; *iii*) the distance between the graphene sheet and back-gate  $b$  and, importantly, *iv*) device temperature  $T$ , due to the coexistence of thermally activated  $n$ - and  $p$ -type carriers at the interface. For any working condition ( $n$ ,  $T$ ), we find that lateral  $p$ - $n$  junctions are generally sharper in devices where metal-graphene interfaces are embedded in environments with low dielectric constants  $\epsilon$  both above and below graphene, whereas distances  $b$  between graphene and back-gate do not significantly alter  $w$ . Temperature effects are more relevant for smaller potential barriers  $\Delta E$ , with  $w$  tending to decrease for higher  $T$ . Also, we discuss favorable device architectures in order to obtain sharper  $p$ - $n$  junctions at room temperature (RT) and demonstrate that sharp junctions with  $w \leq 10$  nm are indeed achieved at RT using non-encapsulated graphene supported on dielectric substrates with low permittivity such as SiO<sub>2</sub> or hexagonal boron nitride, hBN. Finally, we show how the precise details at the metal-graphene interface (such as separation distance  $t_d$  and the dielectric constant of that interface



$\varepsilon_d$ ) are critical to define the  $p$ - $n$  junction in terms of both  $w$  and  $\Delta E$ . This is due to two simultaneous contributions to the total electric field occurring at these positions including the electric field present between metal and graphene layers responsible of creating the  $p$ - $n$  junction; and the large out-of-plane electric field existing between these generated  $p$  and  $n$  regions. As demonstrated below, such interplay may promote the utilization of anisotropic thin dielectrics between metals and graphene to further control  $w$ .

We note that our results can be extended to other 2D materials since they are also doped by the presence of metal clusters [41,42] and are relevant to other applications where the spatial extent of lateral  $p$ - $n$  junctions is important including graphene-metal contacts [36-39] and metal-graphene photodetectors [43,44]. The paper is organized as follows. In Section 2 the electrostatic model is presented. In Section 3 we show results of the junction width  $w$  estimated in lateral  $p$ - $n$  junctions created at metal-graphene interfaces for different device parameters such as gate voltages  $V_g$ ,  $\Delta E$ ,  $\varepsilon$ ,  $b$ ,  $t_d$ ,  $\varepsilon_d$  and  $T$ , and discuss device architectures promoting the formation of sharp  $p$ - $n$  junctions at room temperature. Lastly, we present our conclusions in Section 4.

## 2. Electrostatic model of $p$ - $n$ junctions at metal-graphene interfaces.

When establishing lateral  $p$ - $n$  junctions in 2D materials [3,6,7], a redistribution of charge occurs across the  $p$ - $n$  interface to align the Fermi levels in both  $p$ - and  $n$ - regions while an in-plane potential  $\phi$  with step height  $\Delta\phi$  is established in the materials' plane ( $z = 0$ ) with a junction width  $w$ . Here,  $\Delta\phi$  balances the difference between the intrinsic chemical potentials of the two regions, which are in thermal equilibrium. Solving the problem for a circular  $p$ - $n$  junction with radius  $R$  in cylindrical coordinates  $(r, \phi, z)$  and having rotational symmetry along the azimuthal angle  $\phi$ , the exact spatial distribution of the electrostatic potential  $\phi(r, z)$  and thereby the width of the junction

$w$  can be obtained by solving the following non-linear 2D Poisson equation with appropriate boundary conditions (BC) in a convenient simulation region:

$$-\nabla \mathbf{q} [\varepsilon(r, z) \nabla \phi(r, z)] = \rho_{free}(\phi) \quad (\text{Eq. 1}).$$

It is important to emphasize that this expression of the Poisson equation is able to account for the presence of the back gate in the device through the free charge density  $\rho_{free}$ , the effect of the surrounding media via the local dielectric constant  $\varepsilon$  and the screening produced by the metal island via convenient boundary conditions.

Three specific quantities have to be considered in the case of gate-tunable lateral  $p$ - $n$  junctions created at the interface between graphene regions underneath and outside a circular metal island in the device configuration shown in Fig. 2a. First, the generated in-plane electrostatic potential step  $\Delta\phi$  should be equal to the energy shift  $\Delta E \equiv -\Delta\mu = q\Delta\phi = \mu_g^{(m)} - \mu_g^{(0)}$  resulting from the charge redistribution at these one-dimensional interfaces [33,37,45], where  $\mu_g^{(m)}$  and  $\mu_g^{(0)}$  are the chemical potential in the graphene on the left ( $L$ ) and right ( $R$ ) regions, i.e. underneath and outside the metal (Fig.2b), respectively (situated far away from the  $p$ - $n$  junction interface,  $r = R$ ) and  $q$  is the elementary charge. In other words, there will be a negative or positive energy shift for  $n$  and  $p$  doping, respectively. Second, the free density charge across the junction is given by  $\rho_{free} = \frac{\sigma(\phi)}{t_G}$  inside the graphene layer (zero outside), where  $\sigma$  and  $t_G$  are the surface charge density and the thickness of graphene, respectively. Here, the profile of the surface charge density  $\sigma(r) = q(p(r) - n(r))$  is a consequence of both, the electrostatic gating due to the back gate potential  $V_g$  tuning the overall Fermi level  $E_F$  within the entire graphene device and the asymmetry of the chemical potential along the graphene sheet due to the presence of the metal island (Fig. 2b).

Importantly,  $\sigma$  accounts for all mobile charges in graphene, electrons and holes with corresponding densities  $n$  and  $p$  respectively, coexisting across graphene's  $p$ - $n$  interfaces at finite temperatures  $T$ . Third, the remaining device architecture is accounted for by the permittivity parameters  $\epsilon_1, \epsilon_2$  (Fig. 2b). Unless otherwise stated, we consider a non-encapsulated graphene device (Fig. 2a) supported on a dielectric of relative permittivity  $\epsilon_2 / \epsilon_0 = 3.9$  (value corresponding to SiO<sub>2</sub> and/or hBN dielectric constants, commonly used in experiments [13-17]) and immersed in an environment of permittivity  $\epsilon_1$  equal to the vacuum permittivity  $\epsilon_0$ . The separation distance from the graphene sheet to the back gate is  $b$ , effectively defining the thickness of the dielectric medium with permittivity  $\epsilon_2$  (Figs. 2a,b). The metal-graphene interface is represented [32,37,45] by a dipole layer formed as a result of the charge redistribution in the system within a common equilibrium separation distance  $t_d = 0.3$  nm [32,45] with a permittivity  $\epsilon_d = \epsilon_0$ . Additional details on how to obtain  $\Delta\phi$  and numerically solve  $\phi(r, z)$  with appropriate boundary conditions (BC) in a convenient simulation region are described in Supporting Information Notes 1- 4. We anticipate that *i*) graphene cannot be considered as a perfect metal due to its low carrier density (i.e. quantum capacitance effects should be considered, see Supporting Information Note 4) and *ii*) non-linear screening effects [28] beyond the Thomas-Fermi approximation [46,47] should be taken into account in the system since the characteristic lengths over which the potential varies across junctions formed at metal-graphene interfaces are smaller than  $\lambda_F$ . Also, *iii*) the actual potential of the metal island in this setup (Fig 2a) is constant but unknown, determined by the amount of charge existing in the island [33]. Besides, for completeness, *iv*) we note that our model is valid when the interaction between graphene and metals preserves the bandstructure of graphene [45]. Specific examples of metals and metal-graphene interfaces fulfilling this key condition are reported in Supporting Information Note 5.

Importantly, the possibility to solve Eq.1 without relying on restrictive hypothesis [7] and including (long-range) Coulomb interactions from both metal island and back gate [28,48] are key to simulate the electrostatics of metal-graphene interfaces in graphene field-effect devices, obtain accurate calculations of both potential profile  $\phi(r)$  and/or charge distribution  $\sigma(\phi(r))$  and extract critical quantitative parameters such as  $w$  in the graphene sheet.

Fig. 2c shows both the simulated profile of the potential energy  $-q\phi(r)$  and the energy shift  $\Delta E \equiv -\Delta\mu = \mu_g^{(m)} - \mu_g^{(0)}$  within the graphene plane along a lateral  $n$ - $p$  junction, where the Fermi level is taken as reference ( $E_F = 0$ ). The calculation is undertaken at room temperature ( $T = 300$  K), using a metal that  $n$  dopes graphene with  $\Delta E = -0.2$  eV (close to values given by Ti or Ca [15,49,50], see Supporting Information Note 3) and considering the graphene sheet placed on a  $b = 300$  nm thick layer of  $\text{SiO}_2$ . Furthermore, this calculation is done for a symmetrically doped (bipolar)  $n$ - $p$  junction at the specific back-gate voltage  $V_g$  where the overall Fermi level  $E_F = \Delta E / 2$  (see Supporting Information, Note 3). In our study, the extraction of  $w$  is done by tracing and extrapolating the slope of the curve  $-q\phi(r)$  at the Fermi level up to the step  $\Delta\mu = -q\Delta\phi$ , as commonly done in literature [13]. Other reported ways to obtain  $w$  are given by the width at which the 10% - 90% of the potential step is reached [14], which produces similar results.

The potential  $\phi(r)$  mimics a Fermi function step with a width  $w \sim 8$  nm, in agreement with the creation of sharp  $p$ - $n$  junctions ( $w \leq 10$  nm) at metal-graphene interfaces in graphene field-effect devices. This width is considerably shorter than those reported by combinations of bottom-, top- and/or split-gates even when using thin dielectrics [12-14,24,25,38] ( $w \geq 20$  nm in all cases). Variations of  $w$  for different device parameters including  $\Delta E$ ,  $\epsilon$ ,  $b$ ,  $T$ ,  $t_d$ ,  $\epsilon_d$  and the presence of

asymmetrically doped junctions at different gate-voltages  $V_g$  (i.e carrier concentrations  $n$ ) are discussed in the next section.

### 3. Width of lateral p-n junctions at metal-graphene interfaces: back-gate voltage, potential barrier, device geometry and temperature dependences.

Figure 3a shows the dependence of the junction width  $w$  for different back-gate voltages  $V_g$ . All other device parameters (metal) and environmental conditions ( $T, t_d, \varepsilon_d, b$ ) were similar to those of Fig. 2c. In general, these simulations correspond to asymmetric junctions in both bipolar  $n$ - $p$  (blue shade) and unipolar  $p$ - $p'$ ,  $n$ - $n'$  (gray shade) regimes with Fermi levels placed between, above or below the potential step  $\Delta E$ , respectively [21,39] (see Supporting Information Note 3). A decrement of  $w$  from 12 nm to 5 nm is observed in the entire simulated range of  $|V_g|$  from 0 to 50 V, respectively. From a physical point of view, the increase of  $w$  when decreasing  $n$  (or  $|V_g|$ ) is a consequence of the low density of states ( $DOS$ ) of graphene near the Dirac point [3]. In particular, one can analytically estimate (Supporting Information Note 4 and Ref. [3]) that  $w$  should be proportional to  $1/DOS \sim n^{-1/2}$ , in good agreement with the trend shown in Fig. 3a.

Furthermore, as indicated in the figure by a continuous green line, these values of  $w$  are well below the density-dependent Fermi wavelength  $\lambda_F$  of the charge carriers in the device, thus the created lateral junctions are sharp for any  $n$ .

Fig. 3b shows  $w$  for a symmetric dipolar  $n$ - $p$  junction ( $E_F = \Delta E / 2$ , carrier concentration  $n \sim 1 \times 10^{12} \text{ cm}^{-2}$ ) at  $T = 300\text{K}$  for distances  $b$  between the graphene sheet and the back gate varying from 10 to 400 nm. The latter values are commonly used in devices reported in literature [11-15,38,49]. Whereas it has some dependence on  $b$ ,  $w$  does not considerably increase within the calculated

range for the here considered potential step  $\Delta E = -0.2\text{V}$ . All obtained values of  $w$  are well below the corresponding  $\lambda_F$  in the simulated case  $\sim 35\text{ nm}$ , and the created lateral junctions are therefore sharp in these cases. The absence of a major dependence of  $w$  with respect to  $b$  is ascribed to the effective screening of the out-of-plane electric field in the  $n$ - $p$  junction by the metal island situated on top of (and extremely close to) the graphene layer.

Next, Fig. 3c displays  $w$  for a symmetric dipolar  $n$ - $p$  junction ( $E_F = \Delta E / 2$ , carrier concentration  $n \sim 1 \times 10^{12}\text{ cm}^{-2}$ ) at  $T = 300\text{K}$  and  $b = 300\text{ nm}$  for different relative dielectric constants of the supporting substrate  $\epsilon_2 / \epsilon_0$ . The simulated relative permittivity values  $\epsilon_2 / \epsilon_0$  (1-100) are those present in common devices in literature [11-15], ranging from freestanding graphene ( $\epsilon_2 / \epsilon_0 = 1$ ), graphene supported on  $\text{SiO}_2$  or  $\text{hBN}$  ( $\epsilon_2 / \epsilon_0 = 3.9$ ), or ‘high- $k$ ’ gate oxides such as  $\text{HfO}_2$ ,  $\epsilon_2 / \epsilon_0 \sim 25$  or  $\text{TiO}_2$ ,  $\epsilon_2 / \epsilon_0 \sim 80$ . In general,  $w$  is narrower for smaller  $\epsilon_2 / \epsilon_0$ , increasing notably when increasing  $\epsilon_2 / \epsilon_0$  from 6 to 90 nm within the simulated range for the considered potential step  $\Delta E = -0.2\text{V}$ . Specifically, substrates with  $\epsilon_2 / \epsilon_0$  below 10 show values of  $w < 10\text{ nm}$  (sharp junction case). In contrast ‘high  $k$ ’ dielectrics show widths  $w \geq 50\text{ nm}$  which are already larger than the corresponding  $\lambda_F \sim 35\text{ nm}$  of the charge carriers. From a physical point of view, the increase of  $w$  with use of media of higher permittivity can be understood from two linear contributions resulting from *i*) the dimensionality of lateral  $p$ - $n$  junctions and *ii*) the fact that graphene is not a perfect metal. Specifically, *i*) surrounding dielectric media with higher permittivity makes the large out-of-plane electric field existing at lateral  $p$ - $n$  junctions to vary more slowly, leading to a less efficient screening of such electric field (see Eq.1) and enlarging the width of the  $p$ - $n$  junction. Besides, *ii*) quantum capacitance contributions may have to be considered at metal-graphene interfaces since graphene is not a perfect metal (as aforementioned in Fig.3a). In both cases, the length by which fields penetrate graphene at both sides of the junction shows a linear contribution to the permittivity

of the surrounding medium (see Ref. [6] and Supporting Information Note 4 for further information about contributions *i*) and *ii*), respectively). From a technological perspective, this result shows that the utility of ‘high  $k$ ’ dielectrics for electron optics applications might not be optimal (see detailed discussions below). Furthermore, we note that this observed dependence promotes the utilization of non-encapsulated over encapsulated devices to achieve sharper  $p$ - $n$  junctions at metal-graphene interfaces. This is due to the fact that in encapsulated systems  $\varepsilon_1 > \varepsilon_0$ , increasing thus the overall effective dielectric constant of the device  $\varepsilon_{eff} = (\varepsilon_1 + \varepsilon_2) / 2$  and subsequently enlarging  $w$ , too [6]. Similar conclusions may apply in electron optics devices fabricated via conventional bottom-, top- or split- gates: here, suspended devices [12] would be preferred to achieve sharper  $p$ - $n$  junctions over encapsulated ones [13,14].

Fig. 3d shows the temperature dependence of  $w$  from 10K to 500 K is for two symmetric dipolar lateral junctions ( $E_F = \Delta E / 2$ ) in a device with  $b = 300$  nm. The considered potential steps are  $\Delta E_1 = 0.08$  eV and  $\Delta E_2 = -0.2$  eV, corresponding to carrier concentrations at the junction  $n_1 \sim 3 \times 10^{11}$  cm $^{-2}$  and  $n_2 \sim 1 \times 10^{12}$  cm $^{-2}$  and Fermi wavelengths  $\lambda_{F1} = 65$  nm and  $\lambda_{F2} = 35$  nm, respectively. First, we can see that for any given temperature,  $w$  is smaller for larger potential steps, in particular  $w$  is approximately  $\sim 11$  nm and  $\sim 8$  nm for  $\Delta E_1$  and  $\Delta E_2$ , respectively. Furthermore, when sweeping  $T$ , we note that *i*)  $w$  decreases for higher  $T$  in both cases  $\Delta E_1$  and  $\Delta E_2$  and *ii*) the overall variation of  $w$  ( $|\Delta w| = |(w_{max} - w_{min}) / w_{max}|$ ) is larger for smaller steps  $\Delta E$ . Both interesting trends can be understood due to the influence of thermally activated carriers  $n_{th}$  in the system [3]. In the first case, the larger number of  $n_{th}$  at higher  $T$  will lead to a more efficient screening in the system [28] decreasing thus  $w$ , as commonly observed in conventional semiconductors [51]. Then, thermally activated carriers in a symmetric bias condition will have a larger impact in junctions with smaller

step height, cases where the ratio  $n_{th}/n_l$  is larger: one can see how  $|\Delta w|$  decreases by 30% for  $\Delta E_1$  when increasing the temperature up to 400K. Nevertheless, all calculated values of  $w$  are well below the corresponding  $\lambda_F$  in the three simulations, indicating that lateral  $p$ - $n$  junctions remain sharp in the simulated temperature ranges and  $\Delta E$ .

Fig.3e shows the variation of  $w$  with respect to the metal-graphene distance  $t_d$  calculated for symmetric  $p$ - $n$  junctions. Such distance depends not only on the metal type but also on other factors such as the equilibrium configuration [32]. In this case,  $w$  increases when  $t_d$  increases. Specifically, a considerably variation of  $w$  from 7 to 12 nm is observed when increasing  $t_d$  between 0.2 and 1.1 nm. This behaviour is qualitatively similar to the spread of the in-plane electric potential created in semiconductor field effect transistors with local gates, when these gates are separated away from the semiconductor material (see Refs. [52,53] and Supplementary Information Note 6). However, in our metal-graphene case, the potential step of the junction  $|\Delta E|$  will also decrease when increasing  $t_d$  since the energy shift of graphene underneath the metal depends on the actual graphene-metal distance. For instance,  $|\Delta E| = 0.1$  eV when  $t_d = 1.1$  nm, whereas  $|\Delta E| = 0.2$  eV when  $t_d = 0.3$  nm (with all other simulating conditions are similar to those for Fig. 2c). As such, the increase of  $w$  when increasing  $t_d$  will not only be due to the device geometry (Supplementary Information Note 6), but also to quantum capacitance effects playing a role in the system (Supplementary Note 4). Explicitly, when increasing  $t_d$ ,  $|\Delta E|$  and the corresponding carrier concentration to obtain a symmetric dipolar lateral junction  $n^*$  will decrease, too. The latter will also increase  $w$ , as already reported in Fig.3a. Regarding electron-optics applications, we note that all values of  $w$  are well below the corresponding Fermi wavelengths  $\lambda_F$  in the simulated cases, thus, created lateral junctions are sharp in all these cases ( $t_d \leq 1.1$  nm).



Fig. 3f shows the dependence of  $w$  with respect to the relative permittivity at the metal-graphene interface  $\epsilon_d/\epsilon_0$ . This parameter reflects, for instance, possible oxidation effects occurring in some metals at the interface with graphene [49]. Whereas an abrupt decrement of  $w$  from 8.3 to 5.8 nm is observed when increasing  $\epsilon_d/\epsilon_0$  from 1 to 10;  $w$  decreases at a lower rate when  $\epsilon_d/\epsilon_0$  is larger than 10. This overall behaviour can be intuitively understood from the fact that the electric field between metal and graphene (the one responsible of creating the actual  $p$ - $n$  junction) will be more directional (perpendicular to the graphene film) in a medium with a higher permittivity (Eq.1). In this sense, the overall decrease of  $w$  when increasing  $\epsilon_d/\epsilon_0$  seems to follow a qualitative  $(\epsilon_d/\epsilon_0)^{-1/2}$  dependence which, once again, is similar to trends occurring in depletion regions created by local gates in field effect transistors made from conventional semiconductors (see Refs. [52,53] and Supplementary Information Note 6). However, as in the previous case, we note that the potential step of the junction  $|\Delta E|$  at metal-graphene interfaces additionally varies (increases) when increasing  $\epsilon_d/\epsilon_0$ . For instance,  $|\Delta E| = 0.32$  eV when  $\epsilon_d/\epsilon_0 = 80$ , whereas  $|\Delta E| = 0.2$  eV when  $\epsilon_d/\epsilon_0 = 1$  (other simulating conditions are similar to the ones in Fig. 2c). Thus, the increase of  $w$  when increasing  $t_d$  will not entirely be due to the device architecture (Supplementary Information Note 6), but also to quantum capacitance effects playing a role in the system (Supplementary Note 4). Explicitly, when increasing  $\epsilon_d/\epsilon_0$ ,  $|\Delta E|$  and the corresponding carrier concentration to obtain a symmetric dipolar lateral junction  $n^*$  increase, too. Such fact also decreases  $w$ , as already reported in Fig.3a. All values of  $w$  are well below the corresponding Fermi wavelengths  $\lambda_F$  in the simulated cases, and the created lateral junctions are therefore sharp in these cases.

Finally, we emphasize the interesting (opposite) trends exhibited by  $w$  when changing the relative permittivities of the supporting substrate  $\epsilon_2/\epsilon_0$  ( $w$  increases when  $\epsilon_2/\epsilon_0$  increases) and the dielectric existing at metal-graphene interfaces  $\epsilon_d/\epsilon_0$  ( $w$  decreases when  $\epsilon_d/\epsilon_0$  increases). In general, the

electric field between metal and graphene layers responsible of generating the  $p$ - $n$  junction will be more directional (perpendicular to the graphene film) in a medium with a higher permittivity (thus, reducing  $w$ ). Meanwhile, (by virtue of Eq.1) a lower permittivity in all surrounding dielectrics (not only  $\epsilon_2/\epsilon_0$ , but also  $\epsilon_d/\epsilon_0$ ) guarantees the out-of-plane electric field existing between  $p$  and  $n$  sides of the junction to screen in a shorter distance within the graphene plane (thus, reducing  $w$ , too). This interesting interplay suggests the utilization of anisotropic thin dielectrics at metal-graphene interfaces ( $\epsilon_d/\epsilon_0$ ) to custom tailor  $w$ . Specifically, to reduce further  $w$ , these dielectrics should have a large out-of-plane and low in-plane dielectric constants. An example is depicted in Fig. 4, showing the in-plane ( $z = 0$ ) potential energy  $-q\phi(r)$  between the graphene zone under the metal and the zone outside the metal around  $r = R$ , where the thin dielectric used at the metal-graphene interface is anisotropic and has parallel and perpendicular dielectric constants 1 and 50, respectively. With these parameters,  $w = 4.4$  nm, 45% smaller than the one shown in the isotropic case ( $w = 8$  nm, Fig 2c).

#### 4. Conclusions.

In conclusion, we have performed a systematic and realistic study of the electrostatic problem of  $p$ - $n$  junctions generated at metal-graphene interfaces. Junctions created at these interfaces can be sharp ( $< 10$  nm) and thus they can be potentially used in electron-optics applications. Apart from specific details of the metal-graphene interface (such as the separation distance between graphene and metal or the permittivity at this interface), the widths  $w$  of these lateral junctions considerably depend on the device architecture (i.e. dielectric environment) and experimental parameters including both carrier densities in the graphene sheet (i.e. different gate-voltages in the device) and temperature. Interestingly, our results promote the usage of device dielectrics with low permittivities, and higher temperature operation to reduce the width  $w$  of lateral  $p$ - $n$  junctions created at metal-graphene interfaces in graphene field-effect devices. The technological relevance

of metal-graphene interfaces in graphene electronics point towards the realization of systematic experimental studies to improve the understanding of these intriguing interfaces. In particular, several questions remain open in this field including the fine control of the separation distance metal-graphene; the perturbation of graphene's bandstructure due to the presence of metals [32,43] (see Supporting Information Note 5) including the possible creation of defects due to the metal deposition; the effect of metal granularity [54] in the dipole created at metal-graphene interfaces or undesired residual current being injected from the graphene to the metal in some cases (see Supporting Information Note 7). Finally, our results can be extended to other 2D materials [41,42] and are relevant to other applications where the spatial extent of lateral p-n junctions at metal-graphene interfaces is important, including contacts [36-39] and photodetectors [43,44].

**Acknowledgements** We acknowledge stimulating discussions with M. Brandbyge and G. Calogero. This work was supported by the Danish National Research Foundation Center for Nanostructured Graphene project DNRF103, DFF-EDGE (4184-00030) and the Union's Horizon 2020 research and innovation programme (grant agreement No GrapheneCore2 785219) and the Ministerio de Economía y Competitividad under the project TEC2015-67462-C2-1-R. J. E. S. acknowledges support by the European Structural and Investment Funds in the FEDER component, through the Operational Programme for Competitiveness and Internationalization (COMPETE 2020) [under the Project GNESES - Graphenest's New Engineered System and its Implementation Solutions; Funding Reference: POCI-01-0247-FEDER-033566].

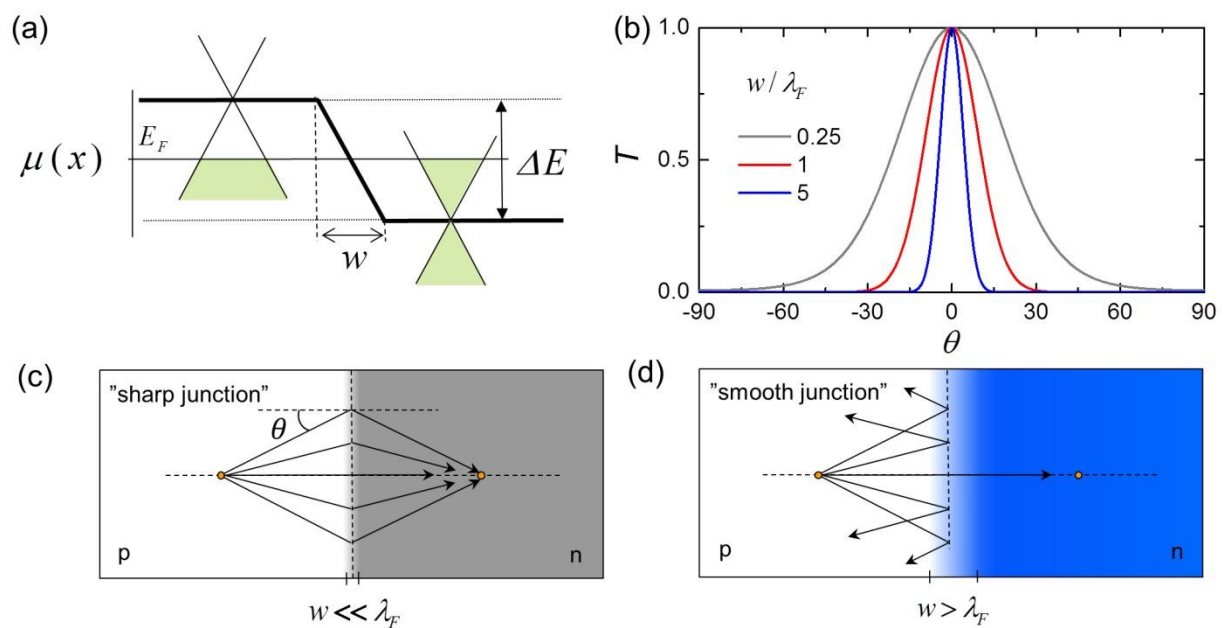


**Figure 1. Lateral  $p$ - $n$  junctions in graphene** (a) Graphene bandstructure near a  $p$ - $n$  junction with a potential step  $\Delta E = -\Delta\mu = q\Delta\phi$  and transition width  $w$ . (b) Angle-selective transmission probability  $T(\theta)$  through a potential step strongly depends on the ratio  $w/\lambda_F$ . (c) Refraction at a sharp  $p$ - $n$  junction with width  $w/\lambda_F \ll 1$  exhibiting Veselago lensing. (d) Same as (b) for a smooth  $p$ - $n$  junction with width  $w/\lambda_F \gg 1$ , leading to ray collimation: rays incident with large  $\theta$  are specularly reflected.

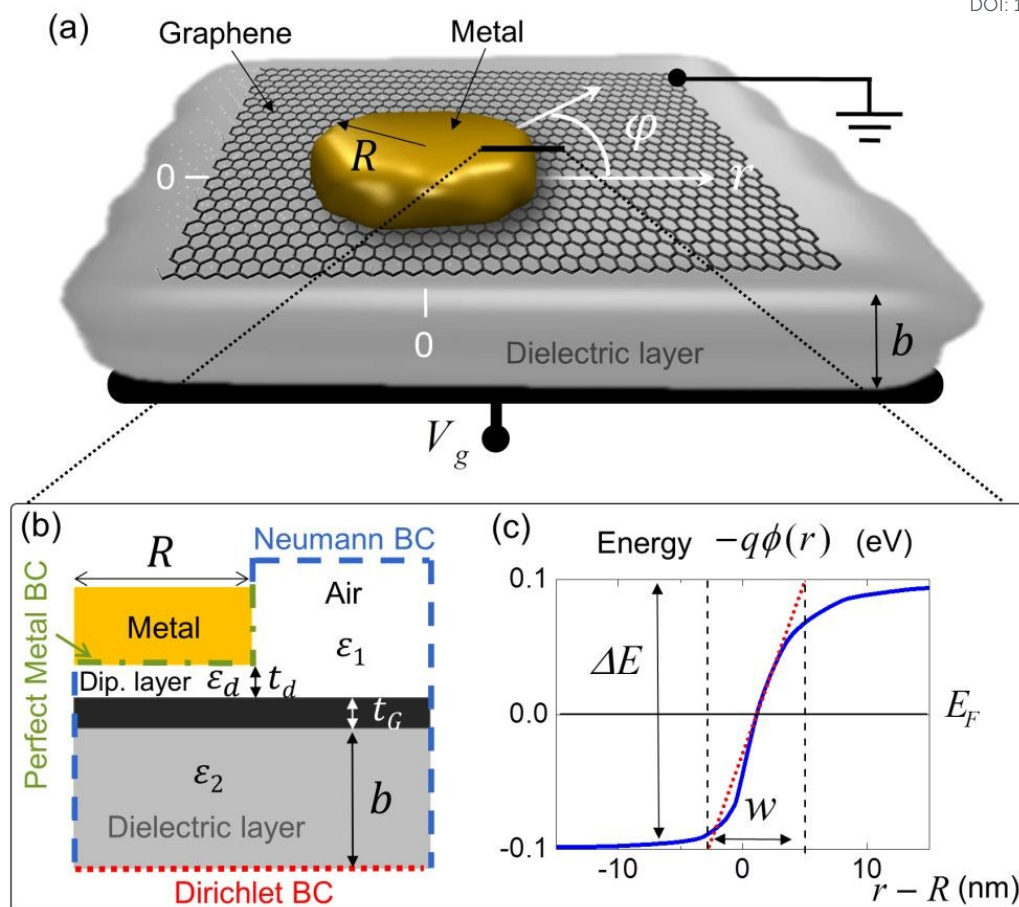


**Figure 2. Sharp lateral  $p$ - $n$  junctions formed at metal-graphene interfaces.** (a) Schematic of a metal island (of radius  $R \sim 50$  nm) deposited on a back gated graphene device.  $p$ - $n$  junctions are formed in graphene at the edge of the metal island. (b) Sketch of the device along the angle  $\varphi = 0$ . Discontinuous lines represent the borders of the calculation region, fulfilling Neumann-like (blue dashes) and Dirichlet boundary conditions (BCs). Specifically, Dirichlet BC with a known potential is applied at the gate electrode (red dots), meanwhile a perfect metal BC is applied at the metal island (green dashed-dotted lines) (Supporting Information, Note 1). (c) In-plane ( $z = 0$ ) potential energy  $-q\phi(r)$  between the graphene zone under the metal and the zone outside the metal around  $r = R$ , with junction width  $w$ . Both  $\phi(r)$  and  $w$  are calculated by iteratively solving Eq.1. The simulation is done at room temperature in cylindrical coordinates around the point  $(0,0,0)$  in order to simulate the circular metal island with radius  $R = 50$  nm. We use Ti as the metal on top of graphene and assuming graphene placed on a 300 nm thick layer of  $\text{SiO}_2$ . We extract  $w$  by the slope at the Fermi level (red dotted line) as commonly done in literature [11]. Our model reflects the fact that Ti  $n$  dopes graphene, in agreement with experiments [15, 49].

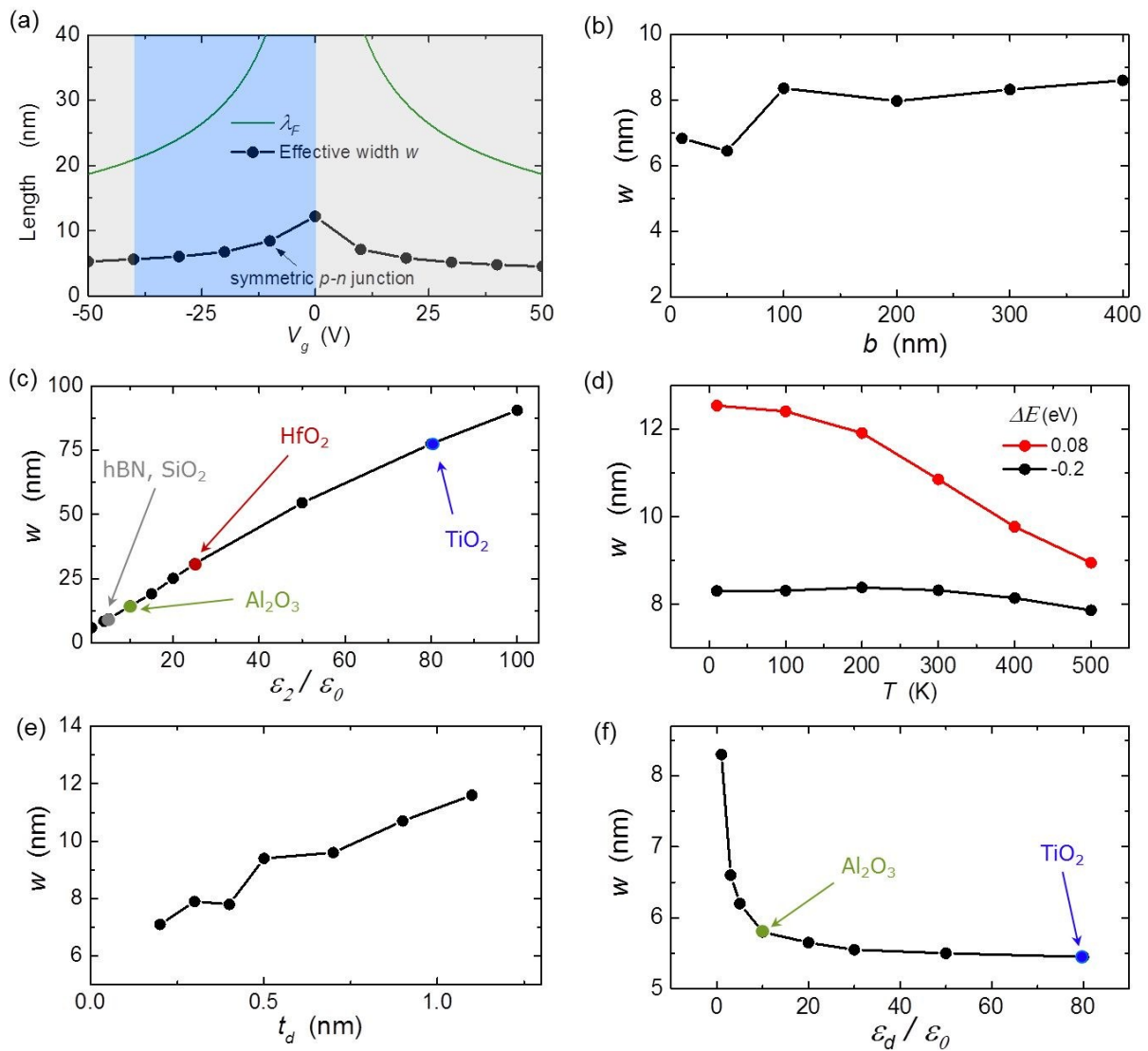


**Figure 3.** Variation of the width  $w$  of lateral  $p-n$  junctions in graphene devices. (a) Dependence of  $w$  on the back-gate voltage  $V_g$  at a constant  $T=300$  K and  $b=300$  nm (Ti is used as metal). Light blue and gray regions correspond to bipolar ( $p-n$ ,  $n-p$ ) and unipolar ( $n-n'$ ,  $p-p'$ ) junctions, respectively. (b) Dependence of  $w$  on the distance to the back-gate  $b$  at  $T=300$  K for a potential step  $\Delta E = -0.2$  eV at  $E_F = \Delta E/2$ . (c) Dependence of  $w$  on the dielectric constant of the supporting substrate  $\epsilon_2$  at  $T=300$  K and  $b=300$  nm for a potential step  $\Delta E = -0.2$  eV at  $E_F = \Delta E/2$ . (d) Dependence of  $w$  on the temperature  $T$  ( $b=300$  nm) for potential steps  $\Delta E = 0.08$  eV (red points) and  $\Delta E = -0.2$  eV (black points) at  $E_F = \Delta E/2$ . (e) Dependence of  $w$  on the metal-graphene distance

$t_d$  at  $T=300\text{K}$  at  $E_F = \Delta E / 2$ . (f) Dependence of  $w$  on the dielectric constant of the metal-graphene interface  $\varepsilon_d$  at  $T = 300\text{K}$  and  $b = 300\text{ nm}$  at  $E_F = \Delta E / 2$ .

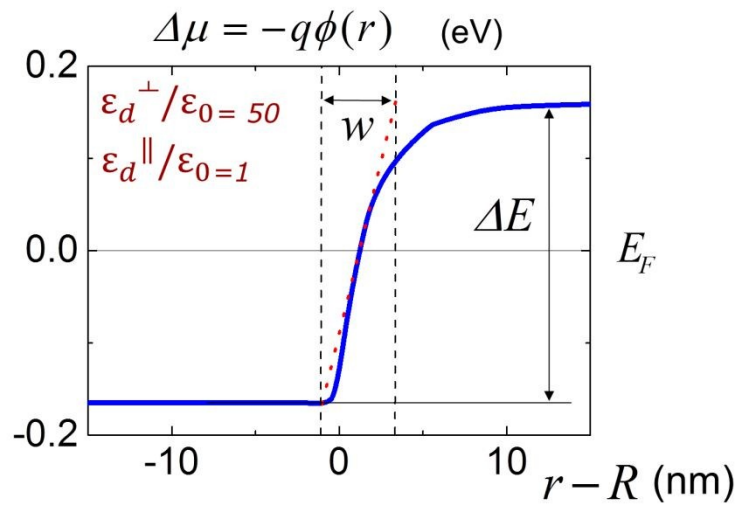


**Figure 4. Width  $w$  of lateral  $p$ - $n$  junctions with anisotropic dielectric constant at the metal-graphene interfaces.** In-plane ( $z = 0$ ) potential energy  $-q\phi(r)$  between the graphene zone under the metal and the zone outside the metal around  $r = R$ , with junction width  $w$  for a metal-graphene interface with anisotropic parallel  $\frac{\varepsilon_d^P}{\varepsilon_0} = 1$  and perpendicular  $\frac{\varepsilon_d^\perp}{\varepsilon_0} = 50$  dielectric constants. In this case,  $w = 4.4\text{ nm}$ , 45% smaller than the one shown in the isotropic case ( $w = 8\text{ nm}$ , Fig 2c).

## References

1. S.M.Sze and K.K.Ng. Physics of Semiconductor devices. *John Wiley & Sons* (2006).
2. C.-H. Lee, G-H. Lee, A.M. van der Zande, W. Chen, Y. Li, M. Han, X. Cui, G. Arefe, C. Nuckolls, T.F. Heinz, J. Guo, J. Hone and P.Kim. Atomically thin p-n junctions with van der Waals heterointerfaces. *Nat. Nanotechnol.* 9, 676 (2014)
3. H.Yu, A. Kutana and B.I. Yakobson. Carrier delocalization in two-dimensional coplanar p-n junctions of graphene and metal dichalcogenides. *NanoLett.*, 16, 5032 (2016)
4. R. Frisenda, A.J. Molina-Mendoza, T. Mueller, A. Castellanos-Gomez and H.S.J. van der Zant. Atomically thin p-n junctions based on two-dimensional materials. *Chem.Soc.Rev.*, 47, 3339 (2018)
5. J. Meng, H-D. Song, C-Z. Li, Y. Jin, L. Tang, D. Liu, Z-M. Liao, F. Xiu and D-P. Yu. Lateral graphene p-n junctions formed by the graphene/MoS<sub>2</sub> hybrid interface. *Nanoscale*, 7, 11611 (2015)
6. A. Nipane, S. Jayanti, A. Borah and J. T. Teherani. Electrostatics of lateral p-n junctions in atomically thin materials. *J.Appl. Phys.* 122, 194501 (2017)
7. F.A. Chaves and D. Jiménez. Electrostatics of two-dimensional lateral junctions. *Nanotechnol.* 29, 275203 (2018)
8. Z.Zhang, P. Chen, X. Duan, K. Zang, J. Luo and X. Duan. Robust epitaxial growth of two-dimensional heterostructures, multiheterostructures, and superlattices. *Science*, 357, 788 (2017)
9. Z-Q. Xu, Y. Zhang, Z. Wang, Y. Shen, W. Huang, X. Xia, W. Yu, Y. Xue, L. Sun, C. Zheng, Y. Lu, L. Liao and Q. Bao. Atomically thin lateral p-n junction photodetector with large effective detection area. *2D Mater.* 3, 041001 (2016)



10. U. Sivan, M. Heiblum, C.P. Umbach and H. Shtrikman. Electrostatic electron lens in the ballistic regime. *Phys. Rev. B* 41, 7935 (1990).
11. J.R. Williams, T. Low, M.S. Lundstrom and C.M. Marcus. Gate-controlled guiding of electrons in graphene. *Nat. Nanotechnol.* 6, 222 (2011)
12. P. Rickhaus, R. Maurand, M-H. Liu, M. Weiss, K. Richter and C. Schönenberger. Ballistic interferences in suspended graphene. *Nat. Commun.* 4, 2342 (2013)
13. G-H. Lee, G-H. Park and H-J. Lee. Observation of negative refraction of Dirac fermions in graphene. *Nat. Physics.* 11, 925 (2015)
14. S. Chen, Z. Han, M.M. Elahi, K.M.M. Habib, L. Wang, B. Wen, Y. Gao, T. Taniguchi, K. Watanabe, J. Hone, A.W. Ghosh and C.R. Dean. Electron optics with p-n junctions in ballistic graphene. *Science*, 353, 1522 (2016)
15. J.M. Caridad, S. Connaughton, C. Ott, H.B. Weber and V. Krstić. An electrical analogy to Mie scattering. *Nat. Commun.* 7, 12894 (2016)
16. A.S. Mayorov, R.V. Gorbachev, S.V. Morozov, L. Britnell, R. Jalil, L.A. Ponomarenko, P. Blake, K.S. Novoselov, K. Watanabe, T. Taniguchi and A.K. Geim. Micrometer-scale ballistic transport in encapsulated graphene at room temperature. *Nano Lett.*, 11, 2396 (2011)
17. L. Wang, I. Meric, P. Y. Huang, Q. Gao, Y. Gao, H. Tran, T. Taniguchi, K. Watanabe, L. M. Campos, D. A. Muller, J. Guo, P. Kim, J. Hone, K. L. Shepard, and C. R. Dean. One-dimensional electrical contact to a two-dimensional material. *Science* 342, 614 (2013)
18. V.V. Cheianov, V. Fal'ko and B.L. Altshuler. The focusing of electron flow and a Veselago lens in graphene *p-n* junctions. *Science*, 315, 1252 (2007)
19. M.I. Katsnelson, K.S. Novoselov and A.K. Geim. Chiral tunneling and the Klein paradox in graphene. *Nat. Phys.* 2, 620 (2006)

20. V.V. Cheianov and V.I. Fal'ko. Selective transmission of Dirac electrons and ballistic magnetoresistance of n-p junctions in graphene. *Phys. Rev. B*, 74, 041403 (2006)
21. P.E. Allain and J.N. Fuchs. Klein tunneling in graphene: optics with massless electrons. *Eur. Phys. J. B*, 83, 301 (2011)
22. F. Libisch, T. Hisch, R. Glattauer, L.A. Chizhova and J. Burgdörfer. Veselago lens and Klein collimator in disordered graphene. *J.Phys.:Cond. Matter*, 29, 114002 (2017)
23. Q. Wilmart, S. Berada, D. Torrin, V. Hung Nguyen, G. Fève, J-M. Berroir, P. Dollfus and B. Placais. A Klein-tunneling transistor with ballistic graphene. *2D Mater.* 1, 011006 (2014)
24. S. Morikawa, Q. Wilmart, S. Masubuchi, K. Watanabe, T. Taniguchi, B. Placais and T. Machida. Dirac fermion reflector by ballistic graphene sawtooth-shaped npn junctions. *Semicond.Sci.Technol.* 32, 045010 (2017)
25. K. Wang, M.M. Elahi, K.M.M. Habib, T. Taniguchi, K. Watanabe, A.W.Ghosh, G-H. Lee and P. Kim. Graphene transistor based on tunable Dirac-fermion-optics. *Proced. Nat. Acad. Sci.* 14, 116, 6575 (2019)
26. P. Bøggild, J.M. Caridad, C. Stampfer, G. Calogero, N.R. Papior and Mads Brandbyge. A two-dimensional Dirac Fermion microscope. *Nat. Comm.* 8, 15783 (2017)
27. G. Calogero, N.R. Papior, P. Bøggild and M. Brandbyge. Large-scale tight-binding simulations of quantum transport in ballistic graphene. *J.Phys:Cond. Matter.* 30, 364001 (2018)
28. L.M. Zhang and M.M. Fogler. Nonlinear screening and ballistic transport in graphene p-n junction. *Phys.Rev.Lett.* 100, 116804 (2008).
29. D. Monroe and J.M. Hergenrother. Challenges of gate-dielectric scaling, including the vertical replacement-gate MOSFET. *AIP Conf. Proceed.* 550, 97 (2001)

30. L. Britnell, R.V. Gorbachev, R. Jalil, B.D. Belle, F. Schedin, M.I. Katsnelson, L. Eaves, S.V. Morozov, A.S. Mayorov, N.M. R. Peres, A. H. Castro Neto, J. Leist, A.K. Geim, L.A. Ponomarenko and K.S. Novoselov. Electron tunneling through ultrathin boron nitride crystalline barriers. *NanoLett.* 12, 117542 (2012)
31. U.Chandni, K. Watanabe, T. Taniguchi and J.P. Eisenstein. Evidence for defect-mediated tunneling in hexagonal boron nitride-based junctions. *NanoLett.* 15, 7329 (2015)
32. G.Giovannetti, P.A. Khomyakov, G. Brocks, V.M. Karpan, J. van den Brink and P.J. Kelly. Doping graphene with metal contacts. *Phys. Rev. Lett.* 101, 026803 (2008).
33. J.E. Santos, N.M.R. Peres, J.M.B. Lopes dos Santos and A.H. Castro Neto. Electronic doping of graphene by deposited transition metal atoms. *Phys. Rev. B* 84, 085430 (2011)
34. C. Gutiérrez, L. Brown, C.-J.Kim, J. Park and A.N. Pasupathy. Klein tunneling and electron trapping in nanometer-scale graphene quantum dots. *Nat. Phys.* 12, 1069 (2016)
35. K.K. Bai, J-J. Zhou, Y-C. Wei, J-B. Qiao, Y-W Liu, H-W. Liu, H. Jiang and L. He. Generating atomically sharp p-n junctions in graphene and testing quantum electron optics on the nanoscale. *Phys. Rev. B*, 97, 045413 (2018)
36. F. Xia, V. Perebeinos, Y-M. Lin, Y. Wu and P. Avouris. The origins and limits of metal-graphene junction resistance. *Nat. Nanotechnol.* 6, 179 (2011)
37. F.A. Chaves, D. Jiménez, A.A. Sagade, W. Kim, J. Riihonen, H. Lipsanen and D. Neumaier. A physics-based model of gate –tunable metal-graphene contact resistance benchmarked against experimental data. *2D Mater.* 2, 025006 (2015)
38. Q. Wilmart, A. Inhofer, M. Boukhicha, W. Yang, M. Rosticher, P. Morfin, N. Garroum, G. Feve, J.-M. Berroir and B. Placais. Contact gating at GHz frequency in graphene. *Sci. Rep.* 6, 21085 (2016)

39. J. Cayssol, B. Huard and D. Goldhaber-Gordon. Contact resistance and shot noise in graphene transistors. *Phys. Rev. B*, 075428 (2009)
40. M.I. Katsnelson, F. Guinea and A.K. Geim. Scattering of electrons in graphene by clusters of impurities. *Phys. Rev. B*, 195426 (2009)
41. T. Komesu, D. Le, I. Tanabe, E.F. Schwier, Y. Kojima, M. Zheng, K. Taguchi, K. Miyamoto, T. Okuda, H. Iwasawa, K. Shimada, T.S. Rahman and P.A. Dowben. Adsorbate doping of MoS<sub>2</sub> and WSe<sub>2</sub>: the influence of Na and Co. *J.Phys:Cond. Matter.*, 29, 28 (2017)
42. Y. Shimazu, K. Arai and T. Iwabuchi. Contact-induced doping in aluminum-contacted molybdenum disulfide. *Jap. J. Appl. Phys.*, 57, 1 (2017)
43. T.J. Etchermeyer, P.S. Nene, M. Trushin, R.V. Gorbachev, A.L. Eiden, S. Milana, Z. Sun, J. Schliemann, E. Lidorikis, K.S. Novoselov and A.C. Ferrari. Photothermoelectric and Photoelectric contributions to light detection in metal-graphene-metal photodetectors. *NanoLett.* 14, 3733 (2014).
44. T. J. Echtermeyer, L. Britnell, P.K. Jasnós, A. Lombardo, R.V. Gorbachev, A.N. Grigorenko, A.K. Geim, A.C. Ferrari and K.S. Novoselov. *Nature Comm.* 2, 458 (2011).
45. G. Giovannetti, P.A. Khomyakov, G. Brocks, V.M. Karpan, J. van den Brink and P.J. Kelly. Doping graphene with metal contacts. *Phys. Rev. Lett.* 101, 026803 (2008).
46. J.M. Caridad, S.R. Power, M.R. Lotz, A.A. Shylau, J.D. Thomsen, L. Gammelgaard, T.J. Booth, A.-P. Jauho and P. Bøggild. *Nature Comm.* 9, 59 (2018)
47. J.M. Caridad, S.R. Power, M.R. Lotz, A.A. Shylau, L. Gammelgaard, A.-P. Jauho and P. Bøggild. *Phys. Rev. B.* (accepted). DOI: 10.1103/PhysRevB.00.005400
48. M.M. Fogler, D.S. Novikov and B.I. Shklovskii. Screening of a hypercritical charge in graphene. *Phys. Rev. B*, 76, 233402 (2007)

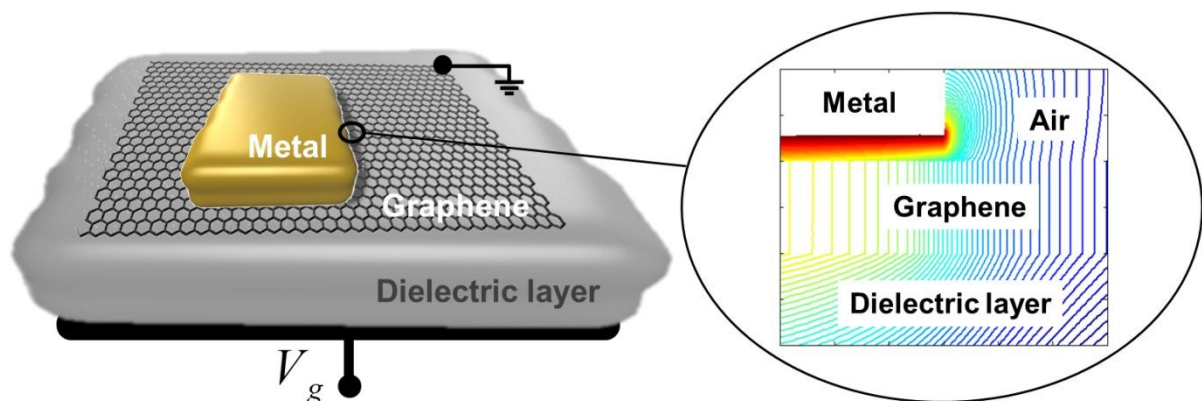
49. M. Zhu, J. Wu, Z. Du, S. Tsang, E.H.T. Teo. Gate voltage and temperature dependent Ti-graphene junction resistance toward straightforward p-n junction formation. *J. Appl. Phys.* 124, 215302 (2018).
50. Q. Ran, M. Gao, X. Guan, Y. Wang and Z. Yu. First-principles investigation on bonding formation and electronic structure of metal-graphene contacts. *Appl. Phys. Lett.* 94, 103511 (2009)
51. S. Paul, R. Lopez, I.L. Repins and J.V. Li. Study of charge transport properties in a ZnO/CdS/Cu(In,Ga)Se<sub>2</sub> solar cell via admittance spectroscopy. *J. Vac. Sci. Tech. B.* 36, 022904 (2018)
52. R-H. Yan, A. Ourmazd and K.F. Lee. Scaling the Si MOSFET: From bulk to SOI to Bulk. *IEEE Trans. Elect. Dev.* 39, 7 (1992).
53. J.P. Colinge. Multiple-gate SOI MOSFETs. *Solid State Electronics* 48, 897, (2004).
54. X. Zhou, A. Kerelsky, M.M. Elahi, D. Wang, K.M. Masum Habib, R.N. Sajjad, P. Agnihotri, J.U. Lee, A.W. Ghosh, F.M. Ross and A.N. Pasupathy. Atomic-Scale characterization of graphene p-n junctions for electron-optical applications. *ACS Nano.* 13, 2, 2558 (2019).

Table of contents entry

View Article Online  
DOI: 10.1039/C9NR02029B

## Electrostatics of metal-graphene interfaces: sharp $p$ - $n$ junctions for electron-optical applications

Ferney A. Chaves<sup>1</sup>, David Jiménez<sup>1</sup>, Jaime E. Santos<sup>2</sup>, Peter Bøggild<sup>3</sup>, José M. Caridad<sup>3†</sup>



Electrostatics of metal-induced lateral  $p$ - $n$  junctions in graphene devices for electron optics applications.